encit 2020

ABCM
Associação Brasileira de Engenharia e Ciências Mecânicas

18th Brazilian Congress of Thermal Sciences and Engineering
November 16–20, 2020 (Online)

ENC-2020-0295
INFLUENCE OF PORE GEOMETRY ASSUMPTIONS OVER THE PLUG-SCALE PERMEABILITY

Vinicius Gonçalves dos Santos
LabCFD - EQ/UFRJ
viniciusgsantos@poli.ufrj.br

Allan Barbosa Geoffroy Motta
Roney Leon Thompson
Vitor Figueirôa Ventura
PEM-COPPE/UFRJ
abg.motta@mecanica.coppe.ufrj.br ; rthompson@mecanica.coppe.ufrj.br ; vfventura1@gmail.com

Jovani Favero
Rodrigo Dias
Wikki Brasil
jovani.favero@wikki.com.br ; rodrigo.dias@wikki.com.br

Luiz Fernando Lopes Rodrigues Silva
LabCFD - EQ/UFRJ
lflopes@eq.ufrj.br

Abstract. *Based on the Continuum Mixture Theory, this work aims to propose a modeling technique to improve the source interaction term between constituents in a mixture of a porous matrix saturated by an incompressible generalized Newtonian fluid. A set of numerical simulations are performed in the pore scale to analyze the dimensionless force behavior for Newtonian and Power-Law fluids, considering many pore geometry idealizations. A wide set of Reynolds number is covered. The results are presented comparing the geometry degree of extension, the fluid model and the pore radius influence. The numerical interaction term is applied for cylindrical pores in plug scale simulations and the permeability field obtained by our assumptions is compared with the permeability obtained analytically. The results are also compared for convergent-divergent pore geometries with the classical cylindrical hypothesis. As the flow rate is kept constant, a significant increase in pressure drop in the plug is noticed when the pores are idealized with a convergent-divergent assumption.*

Keywords: *porous-media, power-law fluid, mixture-theory, pore-scale, plug-scale*

1. INTRODUCTION

Pretroleum is a major source of energy, whose derivatives are of great importance for a large range of industries, such as fuels, plastics and paints. Oil is a Non-renewable resource, and the future perspective of a decline in the worldwide production requires optimization of the production capacity of the know wells. Acid treatment is a widely practiced stimulation technique in oil industry, used to enhance the production rate of reservoirs. The process consists of inserting acid in the well, in order to put it in contact with the reservoir area next to the well walls. When the acid is pumped at lower pressures in order to avoid fracture of the reservoir, the process is named as matrix acidizing.

In matrix acidizing, the acid injected into the porous reservoir reacts with the rocks, creating channels that increase permeability of the media and consequently the flow rate of the oil. The most common acid system used for this purpose is the hydrochloricacid (HCl) due its good reaction rate and low cost, and it is considered that acid system exhibits Newtonian behavior. In highly heterogeneous reservoirs, the use of Newtonian acid systems presents some limitations. The main difficult is the fact that the acid tends to flow in high permeability zones, not reaching other regions of lower permeability. Thus, researches in the last years are focused in the development of other acid systems in order to avoid this problem. Most of these systems exhibit non-Newtonian behavior, with aspects like dependence of shear stress, temperature, concentration and even viscoelastic characteristics.

The dissolution pattern of carbonate reservoirs acidizing is strongly influenced by the injection rate. At intermediate flow rates, there are the formation of long conductive channels known as wormholes. The wormholes pattern provides deep penetration into the carbonate matrix, ensuring the best increase of permeability with the lowest acid injection rate. Different models have been proposed over the past few years, aimed at understanding the phenomena associated with the formation of wormholes. The work of Buijse (1997) has used a single wormhole model of cylindrical tube to represents the wormholes. Other studies like the work of Fredd and Fogler (1998) has used the network model approach to describe reactive dissolution. Network models represent the porous medium as a network of tubes interconnected to each other at the nodes. This model represents the dissolution patterns and qualitative features of dissolution like the optimum flow rate observed in experiments. However, a core scale simulation of the network model is computationally very expensive.

The work of Panga *et al.* (2005) has presented a continuum approach to represent wormhole formation, considering the reaction kinetic and mass transfer aspects. The model describes the dissolution at Darcy's scale, that requires information on the pore scale processes, which are obtained from a pore scale model. Despite of the qualitative results, the model proposed by Panga does not account inertial effects of the fluid it is based on Darcy's Law, valid only to newtonian behavior. Thus, there is a need to modify the model to considering Non-Newtonian acid systems.

A continuum model, initially considering an inert fluid, is considered in this study, in order to allow the use of Generalized Newtonian fluids alongside a complete momentum balance with advective and diffusive terms. The Mixture Theory defined by Atkin and Craine (1976) is the framework used to describe the biphasic system constituted by the acid and the porous matrix. The mixture can be understood as a superposition of a number of continuum media, each one with it's own motion and in each position. That concept allows to make use of more complex equations for the balance of momentum. Usually, a Cauchy momentum equation is applied, with a new source term. This term accounts the internal forces between the constituents of the mixture. In the case of flow through a porous matrix, it accounts the force between the acid and the pore walls. Many constitutive equations were proposed in the literature for that source term, like the ones by (Sampaio and Gama, 1985) and (Mattos and Sampaio, 1993). These equations consider a viscometric geometry for the pore. However, this assumption fails in capture the effect of the contractions and expansions of the fluid that that typically occurs in flow in porous media.

This work is motivated by the applicability in the study of the acidizing, comparing firstly the effect of the different extensional geometries used to represent the pore scale in the source term as well the influence of the Non-Newtonian behavior in the process.

2. METHODOLOGY

2.1 Mixture Theory

The Mixture Theory is a continuum theory that can handle multi-phase problems. The theory is an expansion of the classical Continuum Mechanics (Atkin and Craine, 1976). A mixture consists in two or more deformable materials, each one is considered a continuum. A mixture component is called constituent. Balance equations are postulated in similar way that Continuum Mechanics does. The main distinction is that the influence of a constituent over another must be considered. The mass balance of a constituent of index i can be written in the local form by:

$$\frac{\partial \rho_i}{\partial t} + \nabla \cdot (\rho_i \mathbf{u}_i) = d_i \tag{1}$$

where ρ_i is the constituent density, $\mathbf{u}_i$ is the constituent velocity and d_i is a mass transfer rate that accounts mass interaction between constituents. When there is no chemical reaction, $d_i = 0$. As this term considers internal mass transfer in the mixture, it is required that:

$$\sum d_i = 0 \tag{2}$$

In a similar manner, the balance of momentum for a constituent i in the local and conservative form is written as:

$$\frac{\partial (\rho_i \mathbf{u}_i)}{\partial t} + \nabla \cdot (\rho_i \mathbf{u}_i \otimes \mathbf{u}_i) = \rho_i \mathbf{b}_i + \nabla \cdot \mathbf{T}_i + \mathbf{m}_i \tag{3}$$

where $\mathbf{b}_i$ is the body force and $\mathbf{T}_i$ is the partial Cauchy stress tensor. It is called partial because that it is associated with a constituent and not the phase itself. Similarly, the density refers to the constituent and not the pure phase. The interaction between constituents is represented by the interaction term $\mathbf{m}_i$. It describes the impact over the analyzed constituent by the presence of the others, so the momentum is changed. The modeling of the interaction term is a key feature in the Mixture Theory. As the interaction terms counts for internal forces in the mixture,

$$\sum \mathbf{m}_i = 0. \tag{4}$$

2.2 Flow Through Porous Media

As the flow of a fluid through a porous matrix is a complex phenomena, many theories and models are proposed in the literature. Here, we apply the Theory of Mixtures.

Considering that the volumetric porosity ε is the ratio of the empty volume (or pore volume) over the total volume,

$$\varepsilon = \frac{V_p}{V_t}. \tag{5}$$

The density for the fluid constituent can be connected to the fluid phase by the fraction of fluid occupied in the mixture. Here we consider a single incompressible fluid, so the fluid fills the entire pore space. We also consider that the fluid constituent is described in the equations by the subscript 1. Then, the density of the fluid constituent, ρ_1 is given by:

$$\rho_1 = \varepsilon\rho \tag{6}$$

where ρ is the density of fluid phase. We make the hypothesis that the volumetric porosity is equal to the ratio of pore surface to solid surface. This is true when the porous media is idealized by cylindrical pores. Then, the stress tensor for the constituent 1 can be written as:

$$\mathbf{T}_1 = \varepsilon\mathbf{T} \tag{7}$$

where $\mathbf{T}$ is the Cauchy stress tensor for the fluid phase. For a generalized Newtonian fluid, it can be written as:

$$\mathbf{T} = -p\mathbf{I} + 2\eta\mathbf{D}. \tag{8}$$

p is the mechanical pressure, $\mathbf{I}$ the identity tensor, η the viscosity function and $\mathbf{D}$ is the symmetric part of the velocity gradient. Then, $\mathbf{T}_i$ is given by:

$$\mathbf{T}_1 = -\varepsilon p\mathbf{I} + 2\varepsilon\eta\mathbf{D}. \tag{9}$$

The interaction term must be modeled. An initial approach consists in considering the porous matrix as a array of cylinders, as seen in figure 1.

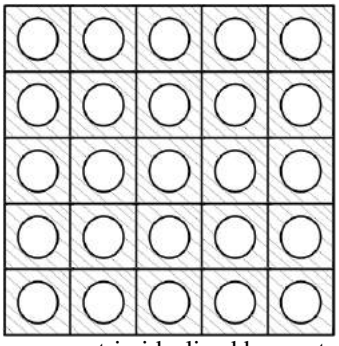

Figure 1: Porous matrix idealized by a set of cylinders

Considering a Hagen-Poiseuille flow inside a cylindrical pore, the mean flow velocity is given by:

$$\bar{u} = -\frac{r_p^2}{8\eta}\frac{dp}{dx} \tag{10}$$

where r_p is the pore radius. The Darcy Law for the superficial velocity of a flow through a porous matrix is given by:

$$\bar{u}_d = \varepsilon\bar{u} = -\frac{1}{\eta}K\frac{dp}{dx}. \tag{11}$$

In equation (11), $\bar{u}_d$ is the Darcy velocity and K is the permeability. Comparing equations (10) and (11), we have:

$$\frac{K}{\varepsilon} = \frac{r_p^2}{8}. \tag{12}$$

Equation 12 is an analytical relation between permeability, porosity and the cylindrical pore radius.

The mean velocity for an incompressible power-law fluid inside a cylindrical pore considering fully developed flow is:

$$\overline{u} = r_p^{\frac{n+1}{n}} \left[\frac{n}{3n+1}\right] \left[-\frac{dp}{dx}\frac{1}{2k}\right]^{\frac{1}{n}}. \tag{13}$$

In equation 13, n is the power-law index and k is the consistency index. Describing the pore radius in function of the Darcy macroscopic properties, the equation (12) applies:

$$\overline{u} = \left[\frac{n}{3n+1}\right] \left[-\frac{dp}{dx}\frac{1}{2k}\right]^{\frac{1}{n}} \left[\frac{8K}{\varepsilon}\right]^{\frac{n+1}{2n}} \tag{14}$$

Considering that the interaction term is balanced by the pressure gradient inside the pores,

$$m_f = \varepsilon \frac{dp}{dx}. \tag{15}$$

We can write equation 14 in function of the pressure gradient $\frac{dp}{dx}$. So, the interaction term is given by:

$$\mathbf{m_f} = -2\varepsilon k \left(\frac{3n+1}{n}\right)^n \frac{\varepsilon}{8K}^{\frac{n+1}{2}} \mathbf{u}^n \tag{16}$$

The interaction term also applies to a Newtonian fluid when $n = 1$ and $k = \eta$. Considering no body force, the set of equations for the fluid constituent when there are no chemical reactions is given by:

$$\frac{\partial(\varepsilon\rho)}{\partial t} + \nabla \cdot (\varepsilon\rho\mathbf{u}_1) = 0 \tag{17}$$

$$\frac{\partial(\varepsilon\rho\mathbf{u}_1)}{\partial t} + \nabla \cdot (\varepsilon\rho\mathbf{u}_1 \otimes \mathbf{u}_1) = -\nabla.(\varepsilon p_1) + \nabla \cdot (2\eta\mathbf{D}_1) - 2\varepsilon k \left(\frac{3n+1}{n}\right)^n \frac{\varepsilon}{8K}^{\frac{n+1}{2}} \mathbf{u}_1^n \tag{18}$$

So the system of equations for the fluid constituent is complete.

2.3 Numerical Interaction Term

There are another ways to analytically obtain the interaction term it is restricted to viscometric idealizations of the pore geometry and simple generalized Newtonian fluid model. More realistic assumptions can be made if we consider a numerical interaction term. The interaction term can be understood as a density of drag force inside the pore. Then, we can define a numerical interaction term by:

$$\mathbf{m}_f = V_t^{-1}\mathbf{f} \tag{19}$$

where $\mathbf{f}$ is the total drag force inside the pores and V_t is the pore volume plus the solid volume, or the total volume. To apply equation (19), we consider that the interaction term is the same over the evaluated mixture. This relation for the interaction term can also be described in function of porosity and the pore volume V_p:

$$\mathbf{m}_f = \varepsilon V_p^{-1}\mathbf{f}. \tag{20}$$

We analyze the influence of the geometry over the drag force inside the pores, so the interaction term is also affected. To do so, we define a convergent-divergent geometry that is defined by the empty space between two identical spheres, as seen in figure (2).

Three parameters are enough to fully describe the geometry, as: the pore entrance radius r_p, the throat radius H and the length l. To compare different idealized pores, the pore volume is kept constant, as the porosity is also maintained constant as a consequence. A cylindrical pore is defined and then we define a set of convergent-divergent pores that match the cylinder volume and length. A parameter δ is defined to describe the percentage of the channel contraption when compared to the cylinder radius:

$$\delta = 1 - \frac{H}{r_p}. \tag{21}$$

When $\delta = 0$, there is no contraption and we recover the cylindrical case. As the parameter is raised, the throat radius H is smaller and the geometry takes a more extensional form.

We aim to cover a set of parameters that engage a range that applies to usual plug scale problem. To achieve that, the drag force is defined as a dimensionless force f^* and it is a function of the Reynolds number:

$$f^* = \frac{f}{4\rho u_c^2 r_p^2} = \hat{g}(Re) \tag{22}$$

Then, a set of forces can be evaluated for a given extension degree δ and a determined fluid model. Here, we analyze Newtonian and Power-Law fluids.

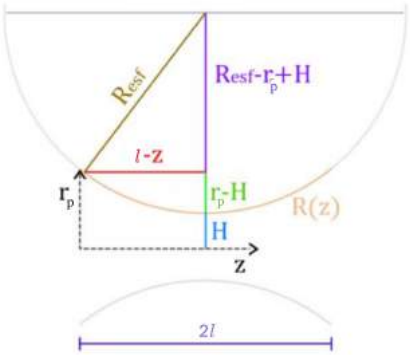

Figure 2: Convergent-Divergent geometry and its parameters (Ventura, 2018).

2.4 Interaction Term and Permeability

In the case where there is no extension, the cylindrical case is recovered. For this case, the permeability can be obtained analytically by equation (12):

$$K = \varepsilon \frac{r_p^2}{8}. \tag{23}$$

The permeability can also be obtained through the Darcy Law for a Newtonian fluid. We rewrite equation 11 in function of permeability:

$$K = -\varepsilon \overline{u} \eta \left(\frac{dp}{dx} \right)^{-1} \tag{24}$$

Another verification can be made when the analytical interaction term (16) is compared to the numerical interaction term (20), so the permeability can be recovered from the fluid model properties and the drag force inside the pore.

2.5 Numerical Formulation

For the solution inside the pores, the following equations for the mass and momentum balance applies:

$$\nabla \cdot \mathbf{u} = 0 \tag{25}$$

$$\rho \frac{D\mathbf{u}}{Dt} = -\nabla p + \nabla \cdot \boldsymbol{\tau} \tag{26}$$

where $\boldsymbol{\tau}$ is the deviatoric part of the stress tensor. The fluid is considered incompressible.

These equations are discretized using the finite volume method. To solve for the pressure, we use the SIMPLE (Semi-Implicit Method for Pressure Linked Equations) algorithm. A stationary solution is of interest. The simulations were performed with the open computational fluid dynamics software OpenFOAM. The mesh were verified so it was guaranteed that the results match the analytical solution in the cylindrical case. In the extensional cases, a very fine mesh was adopted as the reference solution. We apply second order interpolation schemes. The problem considers cyclic boundary conditions.

The results for the permeability in the plug were obtained using equations (17) and (18). For this problem, the PIMPLE algorithm was applied. This algorithm combines features from the SIMPLE and PISO (Pressure-Implicit with Splitting of Operators). It differs from the PISO algorithm allowing more than a single iteration for the outer corrector inside the time loop. The simulations were also performed using OpenFOAM with the finite volume method. The porosity is randomly generated for the initial time step and analytical permeability is a function of porosity.

3. RESULTS

3.1 Pore-Scale Results

The pore-scale simulations were evaluated for a range of parameters suited to the plug scale problem. The parameters analyzed are presented in table (1). We cover a Newtonian fluid, a shear-thinning and a shear-thickening fluid. Also, a wide range of Reynolds numbers are evaluated.

$r_p\ (\mu m)$	1	10	100	-	-
δ	0	0.2	0.4	0.6	0.8
Re	10^{-6}	10^{-4}	10^{-2}	1	-
n	0.5	1	1.2	-	-

Table 1: Range of parameters for the pore-scale cases.

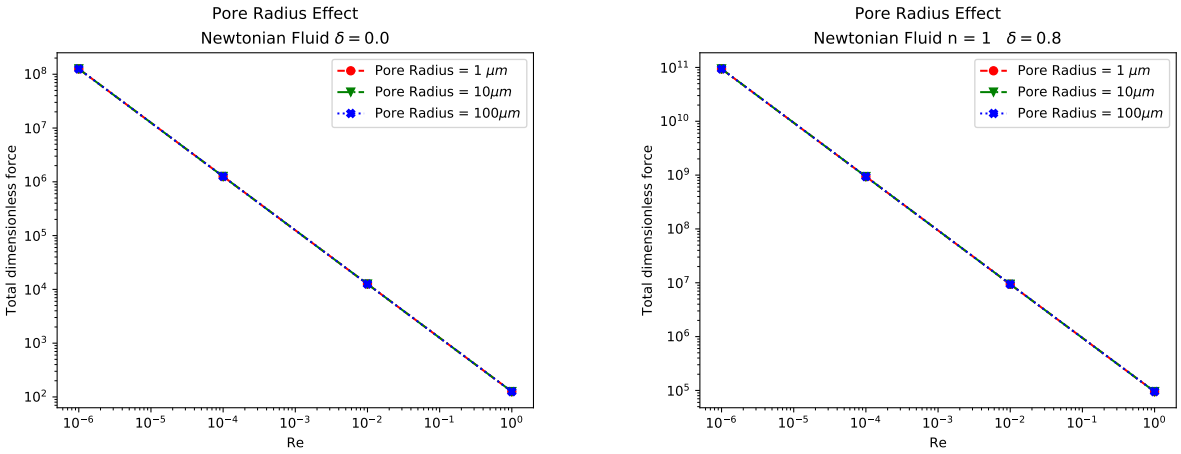

(a) Cylindrical case (b) Convergent-Divergent case with $\delta = 0.8$.

Figure 3: Pore radius influence over the dimensionless force.

We analyze three values for the pore radius r_p. As the Reynolds numbers are kept constant between cases, we verify that the results are the same for all pore radius. Figure (3) compare the cases for the cylindrical case and the most extensional case. No changes in the dimensionless forces are seen, as expected.

Figure (4a) shows the dimensionless force for the Newtonian fluid and different degrees of extension. For the cylindrical case ($\delta = 0$), an analytical solution is possible. It can be seen that the dimensionless force is a linear function of Reynolds for all values of δ. It means that the force is well represented for the dimensionless group, even in high extensions. The cylindrical case also have a good match with the analytical case. From the figure we see that the dimensionless force is raised when δ is increased. This is expected because the extensional geometries have higher contact area between the fluid and the wall. Also, pressure forces are present. The effect is increased when the extension degree is higher.

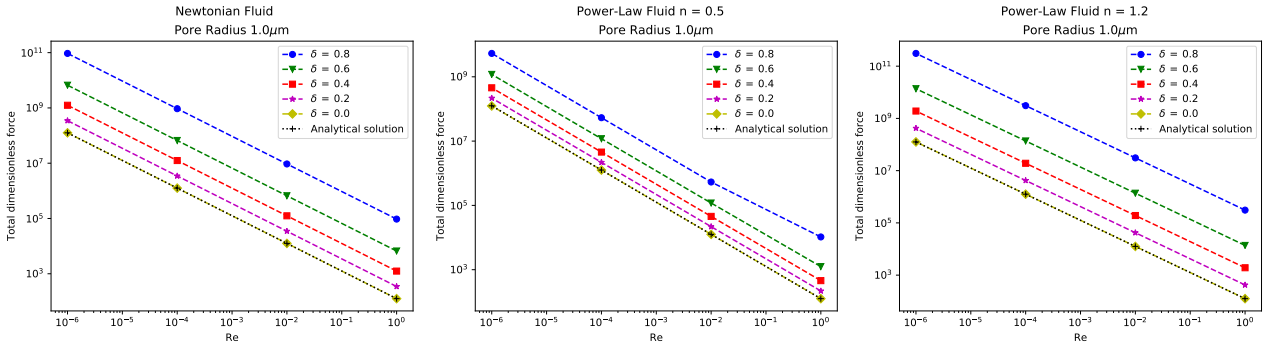

(a) Newtonian cases. (b) Shear-thinning cases. (c) Shear-thickening cases.

Figure 4: Dimensionless force for Newtonian and Power-Law cases.

The Power-Law cases are presented in figure (4b) and (4c). The same trend of Newtonian cases are present. The slope of the curve is changed for the highest number of Reynolds and $n = 0.5$. The flow regime can be changed inside the pore, as this is a case far from the Newtonian case and the velocity is significantly high for a pore-scale problem. This case is not investigated further because higher numbers of Reynolds are of no interest for practical plug problems. The same effect is not noted in the shear-thickening case. Also, it can be seem from figure (4b) that the difference in the dimensionless forces are still of orders of magnitude, but less than Newtonian and the shear-thickening case.

For a given value of δ, we compare the dimensionless force for the evaluated fluid models in figures (5a), (5b) and (5c). For the cylindrical case, $\delta = 0$, the dimensionless force is the same regardless of the fluid model analyzed. For the convergent-divergent case with $\delta = 0.4$ there is a difference and a tendency that when the value of n is higher, the

dimensionless force is also higher. This tendency is kept for the most extensional case, but the difference between cases is higher.

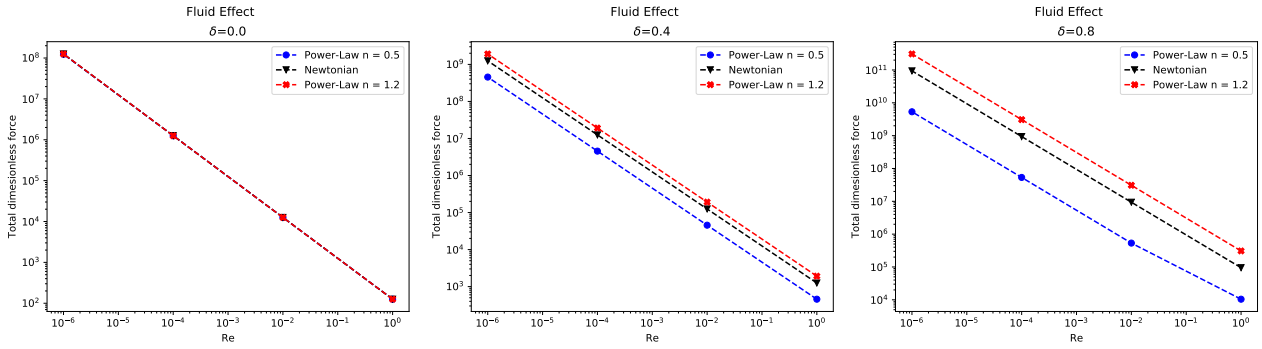

(a) $\delta = 0.0$ (b) $\delta = 0.4$ (c) $\delta = 0.8$

Figure 5: Influence of the parameter n over the dimensionless forces for different degrees of extension.

3.2 Permeability at Darcy Scale

A porosity field was randomly generated for the plug cases. The same porosity field seen in figure (6) is used for all cases. The computational domain is considered bi-dimensional with $7.2\ cm$ length and $3.8\ cm$ height. The analytical permeability field is a function of porosity and pore radius by equation (23). In our cases we establish an average pore radius of $1\mu m$. The initial and boundary conditions for velocity and pressure are presented in table (2).

Variable	Initial Cond.	Inlet	Outlet	Porosity Walls
u	0	$u = u0$	$\nabla u = 0$	slip
p	0	$\nabla p = 0$	$p = 0$	$\nabla p = 0$

Table 2: Initial and boundary condition for the simulated plug cases.

As the velocity and pressure fields are calculated through balance equations based on the Mixture Theory, the numerical interaction term accounts the influence of the porous matrix over the fluid. From the velocity and pressure calculated for each cell, the local permeability is calculated by equation (24). The permeability can also calculated when the numerical interaction term is compared to the analytical interaction term for cylindrical pores, presented in equation (16).

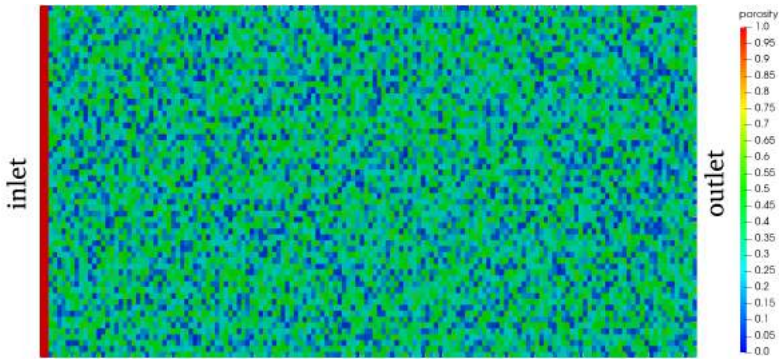

Figure 6: Initial porosity field for all cases.

Permeability is a property of the porous matrix only. So, we verify if the obtained permeability is the same of the analytical case for the fluid models analyzed. Also, we test different inlet velocities so the flow should not have an impact on the results. In figure (7), the comparison for the analytical permeability K, the permeability from Darcy's Law KD and the permeability from the interaction term KA is shown. A good agreement between the numerical permeabilities and the analytical case can be seen. The same pattern is obtained as well as the magnitude.

When the inlet velocity is reduced for $5 * 10^{-5}\ m/s$, the behavior is the same, as expected. A case with even lower velocities is analyzed for $u_0 = 5 * 10^{-6}\ m/s$. Again, the calculated permeabilities show a good match.

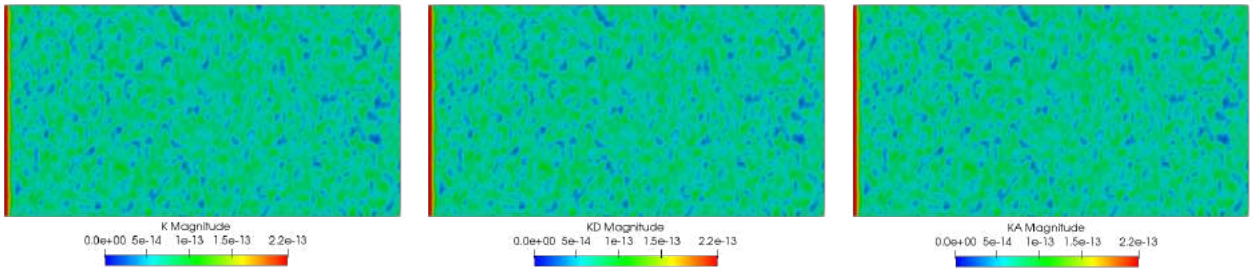

(a) Analytical permeability field. (b) Darcy's permeability field. (c) Interaction term permeability field.

Figure 7: Permeability field obtained through numerical interaction term compared to analytical permeability for inlet velocity of $10^{-4}\ m/s$. Newtonian fluid.

In cases where the fluid model is changed from Newtonian to Power-Law, the permeability still can be calculated from the numerical interaction term for the case with pore with cylindrical geometry. The Darcy's Law no longer applies since it was designed for Newtonian cases. If the Darcy's Law is applied to a power-law case, a modified permeability is obtained, which is not the objective here. From figure (8), the same verification is made for a shear-thinning fluid and the inlet velocity of $10^{-4}\ m/s$. Again, the results show good agreement.

(a) Analytical permeability field. (b) Interaction term permeability field.

Figure 8: Permeability field obtained through numerical interaction term compared to analytical permeability for inlet velocity of $10^{-4}\ m/s$. Shear-thinning fluid with $n = 0.5$.

Finally, another power-law case is evaluated for shear-thickening fluid. Similarly to the shear-thinning case, the validation is made comparing the permeability from the interaction term. We verify that the results also show full compatibility for all tested velocities.

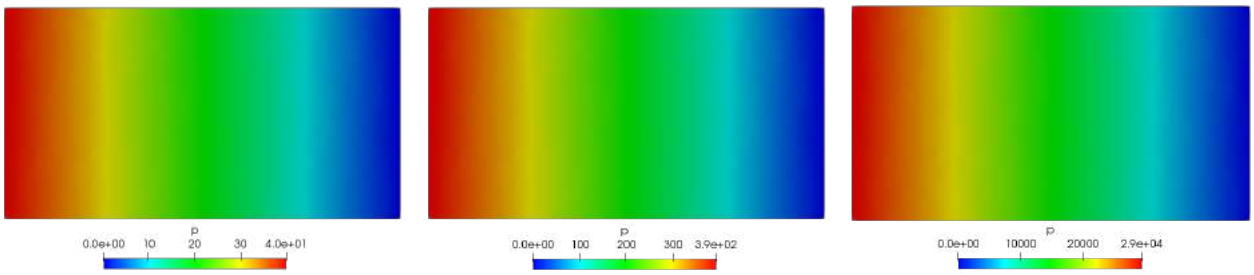

(a) $\delta = 0$. (b) $\delta = 0.4$. (c) $\delta = 0.8$.

Figure 9: Pressure fields for the Newtonian cases with $u = 10^{-4} m/s$.

From figure (4a), a significant difference in the permeability is expected, since the difference in the dimensionless forces between cases is very high. The permeability should be significantly lower for high extensional cases, so the mobility is also lower. This result impacts even Newtonian cases. In figure (9) we compare the pressure field for the Newtonian case with inlet velocity of $u = 10^{-4} m/s$ for three different degrees of extension.

The cylindrical case in (9a) requires the lowest pressure at the inlet. This is expected because the cylindrical assumption is very optimistic. In this case, the pore features a lower resistance to the flow. As the value of δ is increased, the resistance is higher. Thus, the resultant permeability is lower and a higher pressure is necessary to achieve the same flow

rate. We also verify that for the case with $\delta = 0.8$, the pressure is even higher. When compared to the cylindrical case, we see that the pore geometry assumption can have a significant influence over the macroscopic variables in practical problems.

4. CONCLUSIONS

The methodology for the numerical use of the fluid-pore interaction term proved to be effective, since the results of the permeability fields obtained have good agreement with those obtained analytically and, for the Newtonian case, with the Darcy's Law.

The pore scale results showed perfect agreement with the analytical results, available for cylindrical pore geometry. The simulations involving the extension pore geometries show the importance of the discussion about the constitution of the porous medium in the solid-fluid interaction, since the force increases significantly as the pore extension increases. The pore scale simulations also show that the pore radius does not influence the force calculation, with the curves obtained being coincident for the three pore sizes tested. This fact is justified by the dimensionless force procedure, since for in which the value forces are normalized. The pore scale simulations show also that the fluid influence in force value increases with the pore extension.

The applied pore-scale results for different degrees of extension in the plug simulations also have show that the pore idealization can have a significant impact on the macroscopic fields. In this case, the pressure drop was evaluated for Newtonian case with three different degrees of extension and a great difference between the cases was obtained.

The Numerical approach to determine the interaction term proves to be the best way to characterize fluids with more complex rheological behavior, such as the viscoelastics, in which an analytical solution is difficult to obtain even for a cylindrical porous medium.

5. REFERENCES

Atkin, R. and Craine, R., 1976. "Continuum theories of mixtures. basic theory a development". *Quarterly J. Mech. Appl. Math.*, Vol. 29, pp. 209–244.

Buijse, M.A., 1997. "Understanding wormholing mechanisms can improve acid treatments in carbonate formations". *Society of Petroleum Engineers*.

Fredd, C. and Fogler, H.S., 1998. "Influence of transport and reaction on wormhole formation in porous media". *AichE J.*, Vol. 44, pp. 1933–1949.

Mattos, H.C., M.M. and Sampaio, R., 1993. "A thermodynamically consistent constitutive theory for a rigid solid-stokesian fluid mixture". mechanics research communications". *Mechanics Research Communications*, Vol. 29, p. 209.

Panga, M., Ziauddin, M. and Balakotaiah, V., ., 2005. "Two-scale continuum model for simulation of wormholes in carbonate acidization". *Wiley InterScience*, Vol. 51, p. 3248.

Sampaio, R. and Gama, R., 1985. "Relações constitutivas para escoamentos de fluidos não newtonianos através de meios porosos saturados." *Journal of the Brazilian Society of Mechanical Sciences.*, Vol. 7, pp. 267–280.

Ventura, V.F., 2018. "Análise do termo de interação entre o fluido e o meio poroso obtido em teoria de mistura utilizando uma idealização não viscométrica do meio poroso".

6. RESPONSIBILITY NOTICE

The authors are solely responsible for the printed material included in this paper.